Bergische Universität Wuppertal

Fachbereich Mathematik und Naturwissenschaften

Institute of Mathematical Modelling, Analysis and Computational Mathematics (IMACM)

Preprint BUW-IMACM 13/31

Daniel Heubes, Andreas Bartel, Matthias Ehrhardt

Exact Artificial Boundary Conditions for a Lattice Boltzmann Method

November 27, 2013

http://www.math.uni-wuppertal.de

Exact Artificial Boundary Conditions for a Lattice Boltzmann Method

Daniel Heubes*, Andreas Bartel, Matthias Ehrhardt

Bergische Universität Wuppertal, Fachbereich Mathematik und Naturwissenschaften, Lehrstuhl für Angewandte Mathematik und Numerische Analysis, Gaußstrasse 20, 42119 Wuppertal, Germany

Abstract

When using a lattice Boltzmann method on an unbounded (or very large) domain one has to confine this spatial domain to a computational domain. This is realized by introducing so-called artificial boundary conditions. Until recently, characteristic boundary conditions for the Euler equations were considered and adapted to the lattice Boltzmann method.

In this work we propose novel discrete artificial boundary conditions which are derived directly for the chosen lattice Boltzmann model, i.e., on the discrete level. They represent the first exact artificial boundary conditions for lattice Boltzmann methods. Doing so, we avoid any detour of considering continuous equations and obtain boundary conditions that are perfectly adapted to the chosen numerical scheme. We illustrate the idea for a one dimensional, two velocity (D1Q2) lattice Boltzmann method and show how the computational efficiency can be increased by a finite memory approach. Analytical investigations and numerical results finally demonstrate the advantages of our new boundary condition compared to previously used artificial boundary conditions.

Keywords: lattice Boltzmann method, artificial boundary conditions, unbounded domain, D1Q2, characteristic boundary conditions

*corresponding author

Email addresses: heubes@math.uni-wuppertal.de (Daniel Heubes), bartel@math.uni-wuppertal.de (Andreas Bartel), ehrhardt@math.uni-wuppertal.de (Matthias Ehrhardt)

1. Introduction

Numerical methods for *computational fluid dynamics* (CFD) conventionally aim to solve an according model of partial differential equations in terms of macroscopic fluid quantities. Typically, these are equations for the mass density, velocity, pressure and/or temperature, like in the case of the Euler equations or the Navier-Stokes equations. In contrast, when using the *lattice Boltzmann method* (LBM) a mesoscopic description of the fluid is used. This approach is based on a particle model, in which fictitious particles can move with discrete velocities on a prescribed lattice. In LBM, particles with same properties are gathered to *populations*. It is not the evolution of single particles which is considered, but the evolution of these populations. For an introduction to the LBM see, e.g., [1, 2]. The LBM can be applied to a wide range of applications in CFD (e.g., [3]), such as acoustics (e.g., [4]), blood flow (e.g., [5]) or flows with complex physical interactions (e.g., fluid structure interaction [6]).

The boundary conditions in LBM are generally derived from known macroscopic physical conditions, which have to be transferred to the mesoscopic level of populations, e.g., by lifting operator approaches [7]. Now, in simulations often non-physical boundaries occur, e.g., a large fluid domain shall be confined to the most interesting region. These are so-called artificial boundaries and there it is often unclear how to specify boundary conditions, which do not interact with the fluid in an undesired way. This problem appears on both the macroscopic and the mesoscopic scale. For instance, a velocity outflow boundary condition leads to unphysical reflections at the artificial boundary. Ideally, the artificial boundary condition should be chosen such that no spurious effects influence the simulation results.

There exist only a small number of studies for *artificial boundary conditions* (ABCs) for the LBM. Related publications originate from Tekitek et al. [8] as well as Najafi-Yazdi and Mongeau [9]. They both developed an absorbing layer boundary condition with the concept of the *perfectly matched layer* (PML) approach. An alternative approach was proposed in the work of Izquierdo and Fueyo [10], in which they analyze the characteristics of a system for macroscopic quantities. Thus, they are able to construct a system with reduced non-reflecting properties. Solving this system numerically leads to a Dirichlet condition in macroscopic quantities which has to be transferred to the LBM. Recently, this work was extended in [11], where additional terms were taken into account to improve the accuracy of these *characteristic*

boundary conditions (CBCs).

The purpose of the present work is to derive a boundary condition for artificial boundaries on the discrete level. To the author's best knowledge, such results do not exist for the discrete level of LBM yet. The transfer of macroscopic information to the discrete level of populations is always connected with errors. Hence, an exact boundary condition can be derived on the discrete level only. The concept of finite memory allows a very flexible adaptation of the computational effort to the needed accuracy in the ABC.

This article is structured as follows. In Section 2 we discuss a one dimensional LBM with two velocities. In the third section we focus on the evolution of populations. Our derivation can be used to compute populations purely from initial data in a Cauchy problem. This description is used in Section 4 to construct an exact ABC. Furthermore, we derive an efficient approximation of the exact ABC by introducing a history depth (finite memory). Then numerical results are presented in Section 5, which illustrate our findings. Finally, the article is completed by conclusions.

2. The D1Q2 LBM-Model

To study for the first time exact artificial boundary conditions (ABCs), we choose one of the simplest models in LBM. We consider only one spatial dimension with a grid spacing $h > 0$, grid points $x_n = nh$ ($n \in \mathbb{Z}$) and related time points $t_s = sh$ ($s \in \mathbb{N}_0$), defining a regular lattice. The *populations* f_i describe the distribution of fictitious particles moving on that lattice with velocity c_i. By a slight abuse of notation, we employ $f_i(n, s) := f_i(x_n, t_s)$ to denote the populations at the lattice node (x_n, t_s). Here, we consider a two velocity model (D1Q2, notation by [12]) with velocities $c_1 = -1$ and $c_2 = 1$, cf. [13]. The evolution process of the populations is given by the *lattice Boltzmann equation* (LBE):

$$f_i(n + c_i, s + h) = f_i(n, s) - C(f)_i, \quad \text{for} \quad i = 1, 2. \tag{1}$$

The term $C(f)_i$ denotes the collision operator, which models the local particle interaction. Thus, the LBE can be seen as consisting of two basic steps: *collision* (evaluation of the right-hand side) and *streaming/transport* (assignment to left-hand side). For simplicity and feasibility of the proceeding development, we choose a linear model for the *collision operator*:

$$C(f) = \begin{pmatrix} C(f)_1 \\ C(f)_2 \end{pmatrix} = \frac{\omega}{2} \begin{pmatrix} -(a+1) & -(a-1) \\ a+1 & a-1 \end{pmatrix} \begin{pmatrix} f_1 \\ f_2 \end{pmatrix} \tag{2}$$

with parameters $a \in (-1, 1)$ and $\omega \in (0, 2)$. This choice is equivalent to a single time BGK (due to Bhatnagar, Gross and Krook) collision term [14]

$$C(f)_i = -\omega(f_i - E_i),$$

with relaxation parameter ω, equilibrium distribution

$$E_i(\rho) := \frac{1}{2}\rho(1 + ac_i),$$

and *mass momentum* $\rho(n, s) := \sum_i f_i(n, s)$. The equilibrium distribution $E = (E_1, E_2)^\top$ is characterized by

$$C(E)_i = 0. \tag{3}$$

For the LBE (1), we employ a *Chapman-Enskog expansion* [15] with expansion parameter ε. In this way we find the underlying macroscopic evolution equation:

$$\partial_t \rho + a\partial_x \rho = \varepsilon\mu\partial_{xx}\rho + \varepsilon^2\lambda\partial_{xxx}\rho + \mathcal{O}(\varepsilon^3),$$

with parameters

$$\mu := \Big(\frac{1}{\omega} - \frac{1}{2}\Big)\Big(1 - a^2\Big), \qquad \lambda := 2a\Big(\frac{1}{\omega^2} - \frac{1}{\omega} + \frac{1}{6}\Big)\Big(1 - a^2\Big).$$

Let us remark that similar results were obtained by Junk and Rheinländer in [13], in which the model was precisely analyzed using a more general asymptotic expansion. The authors showed that $\rho = \rho^{(0)} + h\rho^{(1)} + h^2\rho^{(2)} + \mathcal{O}(h^3)$ evolves according to an advection equation (up to zeroth order in h) with constant advection velocity a. Higher order terms introduce numerical diffusion. In fact, for an initial profile of the mass momentum $\rho(n, 0) = v_0(n)$, Junk and Rheinländer [13] have shown that it holds:

$$\begin{aligned}
&\partial_t\rho^{(0)} + a\partial_x\rho^{(0)} = 0, && \rho^{(0)}(n, 0) = v_0(n),\\
&\partial_t\rho^{(1)} + a\partial_x\rho^{(1)} = \mu\partial_{xx}\rho^{(0)}, && \rho^{(1)}(n, 0) = 0,\\
&\partial_t\rho^{(2)} + a\partial_x\rho^{(2)} = \mu\partial_{xx}\rho^{(1)} + \lambda\partial_{xxx}\rho^{(0)}, && \rho^{(2)}(n, 0) = 0.
\end{aligned}$$

To simplify the presentation in the current work, we introduce the following abbreviations for the coefficients of the collision operator (2):

$$\alpha = -\frac{1}{2}\omega(1 + a), \quad \beta = \frac{1}{2}\omega(1 - a), \quad \gamma = \frac{1}{2}\omega(1 + a), \quad \delta = -\frac{1}{2}\omega(1 - a). \tag{4}$$

Doing so, we can rewrite the equilibrium condition (3) as

$$0 = \alpha E_1 + \beta E_2, \qquad\qquad 0 = \gamma E_1 + \delta E_2.$$

We note that both equations are equivalent and that they imply

$$E_2 = \frac{1+a}{1-a} E_1. \tag{5}$$

3. Explicit Formula for Several Time Steps

Within this work, the populations f_i denote the *pre-collision* populations, i.e., the populations directly after streaming (of the preceding time step). Furthermore we denote by

$$\tilde{f}_i(n,s) := f_i(n,s) + C(f)_i$$

the *post-collision* populations, cf. (1). In the D1Q2 model with collision operator (2), the populations after one time step can be formulated explicitly:

$$\begin{aligned} f_1(n,s) = \tilde{f}_1(n+1,s-1) &= (1+\alpha) f_1(n+1,s-1) + \beta f_2(n+1,s-1), \\ f_2(n,s) = \tilde{f}_2(n-1,s-1) &= \gamma f_1(n-1,s-1) + (1+\delta) f_2(n-1,s-1) \end{aligned} \tag{6}$$

using abbreviations (4).

In the sequel, we focus on the populations f_1. The populations f_2 can be treated analogously. The deterministic LBE approach of (1) implies that all future populations are uniquely prescribed by the initial populations $f_i^0(n) := f_i(n,0)$ if a Cauchy problem is considered. From (6) we conclude that the population $f_1(n,s)$ is computed by both pre-collision populations from the node $(n+1, s-1)$. These populations themselves are computed from the two populations $f_i(n, k-2)$ as well as the two populations $f_i(n+2, k-2)$. The repeated application of this recursion can be illustrated by a tree as shown in Fig. 1. In this context, we consider this tree as a *directed graph*, where the directions of the edges are positive in time. In Fig. 1 a set of nodes is marked with squares (the sources in the graph). They describe a sufficient set of populations to compute $f_1(n,s)$ (at the node with diamond marker). Furthermore, the set contains no redundant information, since there is no path which connects two sources (a feasible set). Any set of nodes fulfilling both criteria are referred to as a set of *feasible and sufficient* (FaS) nodes. Obviously, given a node (n,s) the set of FaS nodes is not unique; each sub-tree and super-tree with the same leaf (n,s) gives rise to a set of FaS nodes.

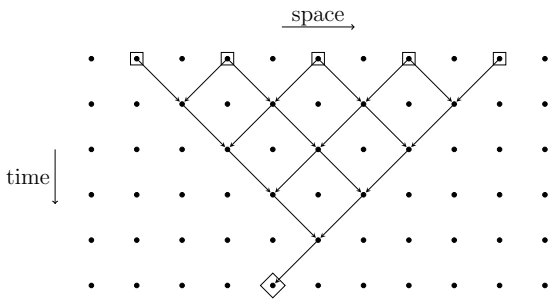

Figure 1: A set of FaS nodes (square marker) and their paths to the node of interest (diamond marker), the leaf (n, s).

Remark 1. The sole dependence on initial populations can be considered as a special case of the above explanation. Thus, any population $f_1(n, s)$ can be computed in terms of given initial populations.

Remark 2. As one can see in Fig. 1, only every second node has a contribution to the node of interest (n, s). Thus, the above D1Q2 model computes the evolution of two separate sets of populations, where information is never exchanged. The two groups of nodes are shuffled in space, such that every second node belongs to the same group. It is possible to completely disregard one group and to combine two subsequent time steps (1) into a single step (with doubled step size and modified collision term). The separation of the two groups can be avoided by including a third population, which corresponds to velocity $c_3 = 0$. This would yield the D1Q3 model.

The population at the node of interest (n, s) can be computed in terms of populations at nodes of a FaS set $\{(m_1, u_1), \ldots, (m_k, u_k)\}$ using some weights $W_i(m_j, u_j)$:

$$f_1(n, s) = \sum_{j=1}^{k} \sum_{i=1}^{2} W_i(m_j, u_j) f_i(m_j, u_j). \tag{7}$$

Since each path $\big($from (m_j, u_j) to $(n, s)\big)$ contributes to the weight, we introduce the set of all such paths $p^j = \{p_1^j, \ldots, p_{\ell_j}^j\}$ and their corresponding

partial weights $W_i(m_j, u_j, p_q^j)$. It holds:

$$W_i(m_j, u_j) = \sum_{q=1}^{\ell_j} W_i(m_j, u_j, p_q^j). \tag{8}$$

Next we discuss these partial weights. They are products of four different terms $1+\alpha$, β, γ and $1+\delta$, cf. (6). For each edge of a path we obtain exactly one factor. Equations (6) express new populations in terms of previous populations: Each leftward arrow – as depicted in Fig. 1 – represents both populations from its origin node, which are needed to express the f_1 population at the destination of that arrow. Analogously, each rightward arrow represents both populations needed for the f_2 population at its destination. In the computation of partial weights, we track for a path only one previous population each, thus we need to pick the corresponding weight factor for the current edge. As (6) states, this factor depends on the previous and current population, hence in the perspective of a path: on the previous and current edge direction. This is visualized in Fig. 2; previous edges are indicated by dashed lines, current edges by solid lines. Now, the partial weight

previous \ current	left	right
left	$1+\alpha$	γ
right	β	$1+\delta$

(a) Table defining the factors

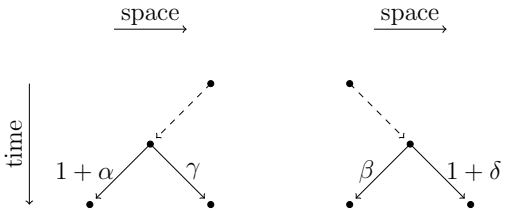

Figure 2: Weight factors. In (b) the previous edge was leftward illustrating the first row of the table (a). In (c) the previous edge was rightward, which represents the second row.

$W_i(m_j, u_j, p_q^j)$ is computed by traversing the path p_q^j edge by edge: To compute the weight $W_1 = W_1(m_j, u_j, p_q^j)$, we start at (m_j, u_j) with the previous fictitious edge having leftward direction (since we track an old f_1 population). To compute the weight $W_2 = W_2(m_j, u_j, p_q^j)$, we add a rightward edge. The factors introduced by each edge (corresponding to the table in Fig. 2) are multiplied.

Example 3. We consider one path from node $(n+1, s-5)$ to (n, s) as shown

in Fig. 3. The corresponding weights are given by

$$W_1 = (1+\alpha)^2 \cdot \beta \cdot \gamma \cdot (1+\delta), \qquad W_2 = (1+\alpha) \cdot \beta^2 \cdot \gamma \cdot (1+\delta).$$

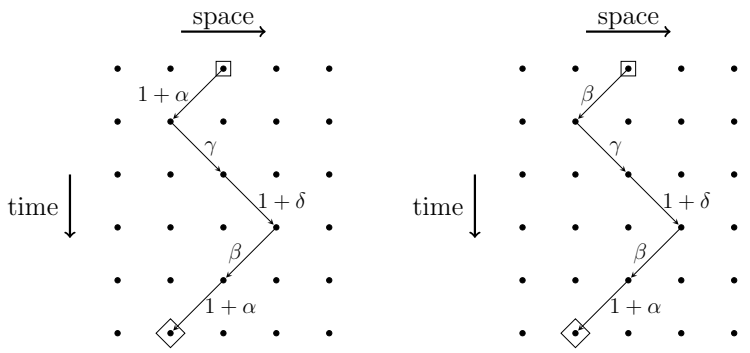

Figure 3: Tree with weight factors: left for the partial weight W_1, right for W_2.

Lemma 4. *Let p^j be a path connecting nodes (m_j, u_j) and (n, s) with length $k = s - u_j$. To compute W_i, let $p^{j,i}$ denote the extension of p^j by a fictitious edge from (a possibly fictitious node) $(m_j - c_i, u_j - 1)$. Let $\bar{v}$ denote the total number of directional changes of $p^{j,i}$ and m denote the number of leftward edges of p^j, for which the previous edge was also leftward. Then we have for the partial weights in* (7) *and* (8)*, respectively:*

$$W_1(m_j, u_j, p_q^j) = (1+\alpha)^m \cdot \beta^{\frac{\bar{v}}{2}} \cdot \gamma^{\frac{\bar{v}}{2}} \cdot (1+\delta)^{k-\bar{v}-m},$$
$$W_2(m_j, u_j, p_q^j) = (1+\alpha)^m \cdot \beta^{\frac{\bar{v}+1}{2}} \cdot \gamma^{\frac{\bar{v}-1}{2}} \cdot (1+\delta)^{k-\bar{v}-m}.$$

Remark 5. a) In the previous Lemma, the last edge of the path $p^{j,i}$ is always leftward, the same holds for the first edge if $i = 1$, hence $\bar{v}$ is always an even number if $i = 1$. On the other hand, if $i = 2$ the first edge of $p^{j,i}$ is of opposite direction than the last edge, therefore $\bar{v}$ is always an odd number if $i = 2$.

b) If one considers (instead of a f_1 population like in (7)) the computation of a new f_2 population and its corresponding weights, the last edge would always be leftward. Modifications to the factors of Fig. 2 are not necessary.

4. Construction of Artificial Boundary Conditions

In the general description of the previous section, we did not consider the presence of boundaries. Without loss of generality there shall be only a right boundary of the computational domain. We assume that this right boundary is located at a lattice point with position x_N. Moreover we assume that there are fictitious nodes in the exterior domain $x > x_N$ and that the corresponding populations are homogeneously initialized in equilibrium, i.e., $f_i^0(n) = E_i$, $i = 1, 2$, for $n > N$.

The task of a (right) boundary condition is to compute $f_1(N, k)$ (inward directed populations) for all $k \in \mathbb{N}^+$. Theoretically, these populations can be computed purely from the initial populations (as FaS set of nodes) using (7). However, this cannot be done efficiently, since the effort for the evaluation of (7) increases rapidly with the number of time steps simulated. In the $k-$th time step a total number of 2^{k-1} different paths has to be considered in the computation of $f_1(N, k)$. Hence, another set of FaS nodes is required. It is reasonable to make use of previously computed populations. Also one should take into account that the exterior domain was initialized homogeneously in equilibrium.

4.1. Boundary adapted set of feasible and sufficient nodes

To compute $f_1(N, k)$, we aim at constructing an expression which depends at most on $f_i(N, \ell)$ with $0 \leq \ell < k$ and on E_i. That is, we consider the tree and set of FaS nodes (marked with squares and triangles) as shown in Fig. 4. Note that due to the initialization of the exterior domain, all the populations within the (dashed) triangle are E_i.

In the following, a superscript A refers to the nodes on the boundary, $x = x_N$ (square nodes in Fig. 4), and a superscript B refers to the exterior equilibrium nodes (triangle nodes). For the required population at the leaf (N, k), we need the number of paths connecting each FaS node with the leaf. Unlike the square nodes, for the triangle nodes, this number depends on time level k. Additionally, the number for all FaS nodes depends on the actual FaS node ℓ and on the number of directional changes (related variable is v).

Given the number of paths P with the same properties p (such as directional changes) from a certain node (m_j, u_j), we can compute the weights (cf. (7)) by

$$W_i(m_j, u_j) = \sum_p P(m_j, u_j, p) \cdot W(m_j, u_j, p),$$

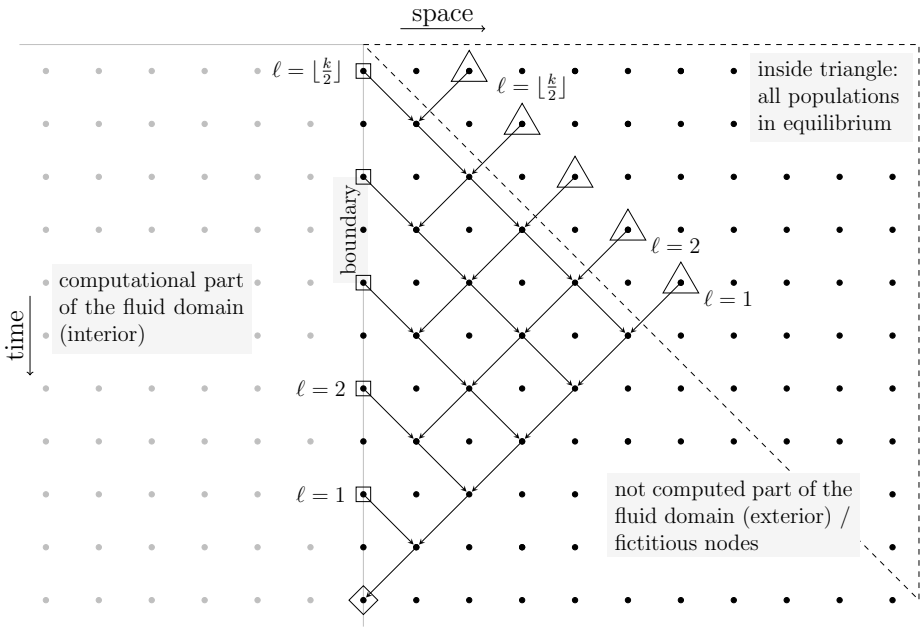

Figure 4: The square (A) and triangle nodes (B) define a set of FaS nodes and are used in the computation of the artificial boundary condition at the diamond node.

provided the weight $W(\cdot, \cdot, p)$ of one path corresponding to $P(\cdot, \cdot, p)$ is uniquely given by the property p. The sum is taken over all possible properties.

Let $P^B(k, \ell, v)$ denote the total number of paths starting in the triangle node $(N + \lfloor \frac{k}{2} \rfloor + 2 - \ell, \lceil \frac{k}{2} \rceil - \ell)$, ending in (N, k) and having $2v$ directional changes, where $\ell = 1, \ldots, \lfloor \frac{k}{2} \rfloor$.

Lemma 6. *For P^B holds:*

a) Provided k is even, $P^B(k+1, \ell, v) = P^B(k, \ell, v)$.

b) $v = 0$ is only possible for the node labeled $\ell = 1$ and we have

$$P^B(k, 1, 0) = 1, \quad k \geq 2. \tag{9}$$

c) The remaining non-zero values are given for $k \geq 4$, $\ell = 2, \ldots, \lfloor \frac{k}{2} \rfloor$ and

$v = 1, \ldots, \ell - 1$:

$$P^B(k, \ell, v) = \left(1 - \frac{\ell - 1}{\lfloor \frac{k}{2} \rfloor}\right) \cdot \binom{\lfloor \frac{k}{2} \rfloor}{v} \cdot \binom{\ell - 2}{v - 1}. \tag{10}$$

Proof. For a) and b), one can inspect Fig. 4. Case c) can be proven by showing that (9) and (10) fulfill the recursion

$$P^B(k, \ell, v) = P^B(k-2, \ell, v) + \sum_{p=1}^{\ell-1} P^B(k-2, p, v-1), \quad \ell = 1, \ldots, \left\lfloor \frac{k}{2} \right\rfloor - 1,$$

$$P^B(k, \ell, v) = \sum_{p=1}^{\ell-1} P^B(k-2, p, v-1), \qquad \ell = \left\lfloor \frac{k}{2} \right\rfloor.$$

The recursion itself can be directly deduced. □

Corollary 7. *The corresponding weights $W_i^B(k, \ell, v)$ are computed as*

$$\begin{aligned} W_1^B(k, \ell, v) &= (1+\alpha)^{\lfloor k/2 \rfloor + 1 - v} \cdot \beta^v \cdot \gamma^v \cdot (1+\delta)^{\ell - v - 1}, \\ W_2^B(k, \ell, v) &= \frac{\beta}{(1+\alpha)} W_1^B(k, \ell, v). \\ &= (1+\alpha)^{\lfloor k/2 \rfloor - v} \cdot \beta^{v+1} \cdot \gamma^v \cdot (1+\delta)^{\ell - v - 1}. \end{aligned} \tag{11}$$

Analogously, let $P^A(\ell, v)$ denote the total number of paths starting in node $(N, k - 2\ell)$ and having $2v - 1$ changes of directions.

Lemma 8. *It holds:*

a) For $\ell = 1$:

$$P^A(1, 1) = 1. \tag{12}$$

b) For $\ell \geq 2$ the remaining non-zero values read:

$$P^A(\ell, v) = \frac{1}{\ell - v} \binom{\ell - 1}{v} \binom{\ell - 2}{v - 1}, \quad v = 1, \ldots, \ell - 1. \tag{13}$$

Proof. One can argue the validity of

$$P^A(\ell, v) = \sum_{p=2}^{\ell} P^B(2\ell - 2, \ell + 1 - p, v - 1),$$

which gives rise to (13). □

Corollary 9. *The corresponding weights are computed as*

$$W_i^A(\ell, v) = (1+\alpha)^{\ell - v} \cdot \beta^v \cdot \gamma^{v+1-i} \cdot (1+\delta)^{\ell - v - 1 + i}. \tag{14}$$

Now, having the number of paths and weights for the set of FaS nodes, the general evolution can be summarized as:

Theorem 10. *For the boundary adapted set of FaS nodes, Fig. 4, the evolution expression* (7) *with* (9)-(14) *is given as*

$$\begin{aligned} f_1(N,1) &= E_1, \\ f_1(N,k) &= \sum_{i=1}^{2} \left(\sum_{\ell=1}^{\lfloor \frac{k}{2} \rfloor} A_i(\ell) f_i(N, k-2\ell) + B_i(k) E_i \right), \qquad k \geq 2, \end{aligned} \tag{15}$$

where

$$\begin{aligned} A_i(1) &= W_i^A(1,1) = \beta \cdot \gamma^{2-i} \cdot (1+\delta)^{i-1}, \\ A_i(\ell) &= \sum_{v=1}^{\ell-1} P^A(\ell, v) \cdot W_i^A(\ell, v), \qquad \ell = 2, \ldots, \left\lfloor \frac{k}{2} \right\rfloor, \end{aligned} \tag{16}$$

$$B_i(k) = W_i^B(k,1,0) + \sum_{\ell=2}^{\lfloor \frac{k}{2} \rfloor} \sum_{v=1}^{\ell-1} P^B(k, \ell, v) \cdot W_i^B(k, \ell, v). \tag{17}$$

Remark 11. Given the assumption that the exterior domain was initialized in equilibrium, the evolution of the inward directed boundary population according to (15) (deduced in Thm. 10) is an *exact artificial boundary condition.*

However, the effort for computing the sums in (15)-(17) increases significantly while proceeding in time. Thus the next step is to modify (15), such that the increasing computational effort can be avoided. This is realized by a truncation of the involved sums.

4.2. Consistency with equilibrium

If all populations are homogeneously initialized in equilibrium, i.e.,

$$f_i^0(n) = E_i, \quad \text{for any} \quad n \in \mathbb{Z} \tag{18}$$

and if there are no boundaries, then the equilibrium will be conserved, due to (3). Thus, a boundary condition should also conserve the equilibrium populations. That is the requirement

$$f_1(N,k) = E_1, \quad \text{for} \quad k \geq 0. \tag{19}$$

The assumption (18) simplifies (15) to the expression:

$$f_1(N,k) = \left(\sum_{\ell=1}^{\lfloor \frac{k}{2} \rfloor} A_1(\ell) + B_1(k) \right) E_1 + \left(\sum_{\ell=1}^{\lfloor \frac{k}{2} \rfloor} A_2(\ell) + B_2(k) \right) E_2. \tag{20}$$

The requirement (19) is fulfilled for (20) if A_i and B_i are computed by (16) and (17). However, the requirement can be used to compute B_i for other values of A_i than (16). To this end, we use the short-hand notation:

$$T_i^A(q) := \sum_{\ell=1}^{q} A_i(\ell). \tag{21}$$

Substituting (5) into (20) yields

$$f_1(N,k) = \left[T_1^A\left(\left\lfloor \frac{k}{2} \right\rfloor \right) + \frac{1+a}{1-a} T_2^A\left(\left\lfloor \frac{k}{2} \right\rfloor \right) + B_1(k) + \frac{1+a}{1-a} B_2(k) \right] E_1.$$

In order to fulfill (19) we derive the condition

$$B_1(k) + \frac{1+a}{1-a} B_2(k) = 1 - T_1^A\left(\left\lfloor \frac{k}{2} \right\rfloor \right) - \frac{1+a}{1-a} T_2^A\left(\left\lfloor \frac{k}{2} \right\rfloor \right). \tag{22}$$

Moreover, (11) implies the relation

$$B_2(k) = \frac{\beta}{1+\alpha} B_1(k). \tag{23}$$

Thus, if the values A_i were not computed by (16) or if the sums (21) in (15) are truncated, then one can compute corresponding values $B_i(k)$ by solving the system (22) and (23).

4.3. Reduction of computational effort by truncation

We consider the exact ABC (15)-(17) and aim at reducing the computational effort. If the boundary population $f_1(N,k)$ depends on a number of $h(k)$ past boundary populations, we refer to $h(k)$ as *history depth* of the boundary condition at time level k. More precisely, $h(k)$ shall indicate that we need the following past time levels:

$$k - 2\ell \quad \text{with} \quad \ell = 1, \dots, h(k).$$

For the populations of the exact ABC we have $h(k) = \lfloor \frac{k}{2} \rfloor$. To reduce the computational effort of the sum in (15), we suggest to use a bounded history depth ("finite memory"):

$$h(k) = \min \left\{ \left\lfloor \frac{k}{2} \right\rfloor, \ H \right\}, \quad H \in \mathbb{N} \text{ fixed.}$$

This truncation strategy is motivated by the following conjecture. For simplicity, in the sequel we abbreviate the full parameter domain for (ω, a) by

$$F := (0,\, 2) \times (-1,\, 1).$$

Conjecture 12. *For any $(\omega, a) \in F$, the $|A_i(\ell)|$ are decaying in ℓ, and it holds*

$$\lim_{\ell \to \infty} A_1(\ell) = 0 \quad \textit{and} \quad \lim_{\ell \to \infty} A_2(\ell) = 0.$$

Lemma 13. *For any $(\omega, a) \in D \cup \tilde{D}$ (see Fig. 5) with*

$$D := \left\{ (\omega, a) \in F \;\middle|\; 1 + |a| \le \frac{2}{\omega} \right\},$$

$$\tilde{D} := \left\{ (\omega, a) \in F \;\middle|\; \left(1 + \sqrt{\frac{(2-\omega)^2 - a^2\omega^2}{(a^2-1)\omega^2}} \right)^2 \le \frac{4}{(1-a^2)\omega^2} \right\}$$

the Conjecture 12 is true.

Proof. The convergence of A_1 implies the convergence of A_2, and vice versa, due to

$$A_2(\ell) = \frac{1+\delta}{\gamma} A_1(\ell),$$

which follows from the definitions (14). We note that β and γ are positive for all $(\omega, a) \in F$, whereas $1+\alpha$ and $1+\delta$ are simultaneously positive only for $(\omega, a) \in D$. The convergence of A_1 can be proven for $(\omega, a) \in D$ by writing $A_1(\ell)$ as

$$A_1(\ell) = [(1+\alpha)(1+\delta)]^\ell \sum_{v=1}^{\ell-1} P^A(\ell, v) \left(\frac{\beta\gamma}{(1+\alpha)(1+\delta)} \right)^v,$$

and applying the general estimate

$$\sum_{v=1}^{\ell-1} P^A(\ell, v) p^{2(\ell-v)} q^{2v} < \frac{(p+q)^{2\ell}}{\ell}, \quad \ell \geq 2, \quad p,\, q \in \mathbb{R}^+. \tag{24}$$

Thus, we obtain

$$A_1(\ell) < \frac{[(1+\alpha)(1+\delta)]^\ell \left(1 + \sqrt{\frac{\beta\gamma}{(1+\alpha)(1+\delta)}}\right)^{2\ell}}{\ell},$$

where the numerator can be shown to be in (0, 1]. Negative values for the weights occur if $(\omega, a) \in F \setminus D$, more precisely, exclusively either $1+\alpha$ or $1+\delta$ is negative. In this case, one can prove the convergence of $|A_i(\ell)|$ by applying the estimate (24) to

$$|A_1(\ell)| \leq [\beta\gamma]^\ell \sum_{v=1}^{\ell-1} P^A(\ell, v) \left| \frac{(1+\alpha)(1+\delta)}{\beta\gamma} \right|^v$$

and proceeding analogously. □

Remark 14. Numerical evidence shows that the decay in Conjecture 12 seems to hold for all $(\omega, a) \in F$, however we have no analytical proof for the the missing part in Fig. 5 ($F \setminus D \cup \tilde{D}$).

In the exact ABC (15) the weights of the boundary populations $f_i(N, k-2\ell)$ are decreasing for increasing ℓ. This is a motivation to disregard populations with large ℓ to obtain an efficient approximation.

When the history depth is truncated, the relation of the previous section has to be used to get a consistent boundary condition. Instead of using (17)

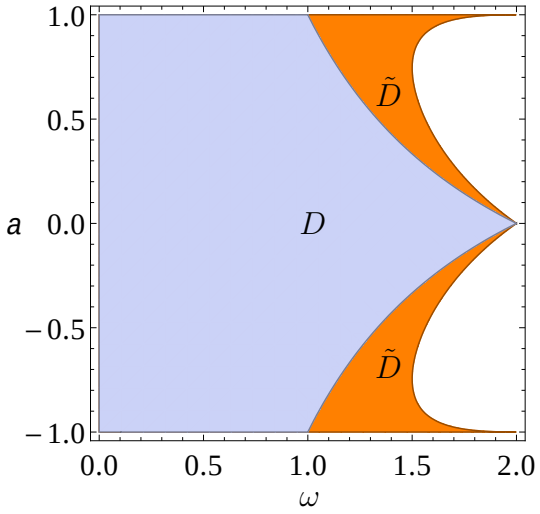

Figure 5: The colored region shows the domain for which $\lim_{\ell\to\infty} A_i(\ell) = 0$ was proven analytically.

the system (22) and (23) has to be solved, which yields explicitly:

$$\begin{aligned} B_1(k) &= \left(1 + \frac{1+a}{1-a}\frac{\beta}{1+\alpha}\right)^{-1} \left(1 - T_1^A\big(h(k)\big) - \frac{1+a}{1-a} T_2^A\big(h(k)\big)\right), \\ B_2(k) &= \left(\frac{1+\alpha}{\beta} + \frac{1+a}{1-a}\right)^{-1} \left(1 - T_1^A\big(h(k)\big) - \frac{1+a}{1-a} T_2^A\big(h(k)\big)\right). \end{aligned} \tag{25}$$

Altogether, the *approximate artificial boundary condition* is given by

$$f_1(N,k) = \sum_{i=1}^{2} \left(\sum_{\ell=1}^{h(k)} A_i(\ell) f_i(N, k-2\ell) + B_i(k) E_i \right), \quad k \geq 2, \tag{26}$$

where the required $A_i(\ell)$ and $B_i(k)$ are computed by (16) and (25), respectively.

5. Numerical Results

Next, we numerically test the approximate ABC (26) and discuss the results. In our test setup, the mass momentum is initialized at $t = 0$ as [13]

$$v_0(x) = \begin{cases} 1 & \text{for} \quad x \leq 0.3, \\ 1 + 0.4 \cdot \exp\left(\frac{-15^{-2}}{(x-0.3)^2}\right) \cdot \exp\left(\frac{-15^{-2}}{(x-0.7)^2}\right) & \text{for} \quad 0.3 < x < 0.7, \\ 1 & \text{for} \quad 0.7 \leq x, \end{cases}$$

such that $v_0 \in C^\infty(\mathbb{R})$. Corresponding populations are initialized via an evaluation of the equilibrium distribution,

$$f_i(n) = \frac{1}{2} v_0(x_n)(1 + ac_i).$$

We consider the spatial interval [0, 1], which is discretized with step sizes $h_1 = 0.025$ and $h_2 = 0.005$. Hence, the computational grid is given by $G_x := \{x_0, x_1, \ldots, x_N\}$ with $N = 1/h_1$ or $N = 1/h_2$. The free parameters are the advection velocity a, the collision parameter ω and the maximal history depth H. For a measurement of the accuracy we compute a reference solution ρ_{ref} by assigning the exact ABC. This is equivalent to a simulation on a sufficiently larger interval than [0, 1]. We measure the accuracy of the approximate ABC by the maximal absolute error:

$$\text{Err}(t) := \max_{x \in G_x} |\rho(x, t) - \rho_{\text{ref}}(x, t)| \,. \tag{27}$$

In the plots below we kept all parameters fixed except for one parameter in each case. By this procedure one can see that the error depends on all parameters. In Fig. 6 the varying parameter is the maximal history depth H and we see that the error is decreasing when we take a larger H (left plot with $h_1 = 0.025$, right plot with $h_2 = 0.005$). Subsequently in Fig. 7, we kept all parameters except for the advection velocity a. The higher the advection velocity, the faster does the initial peak arrive at the artificial boundary. Finally, the plots in Fig. 8 show the dependence on the relaxation parameter ω. The larger the value of ω the smaller absolute errors are observed.

Any acoustic wave or a simple sine wave is composed of peaks and troughs. The above excitation v_0 gives a simple peak. Changing the sign of the factor 0.4 in v_0 results in a single trough. Due to the symmetry, the errors depicted in Figs. 6-8 holds for both initial data.

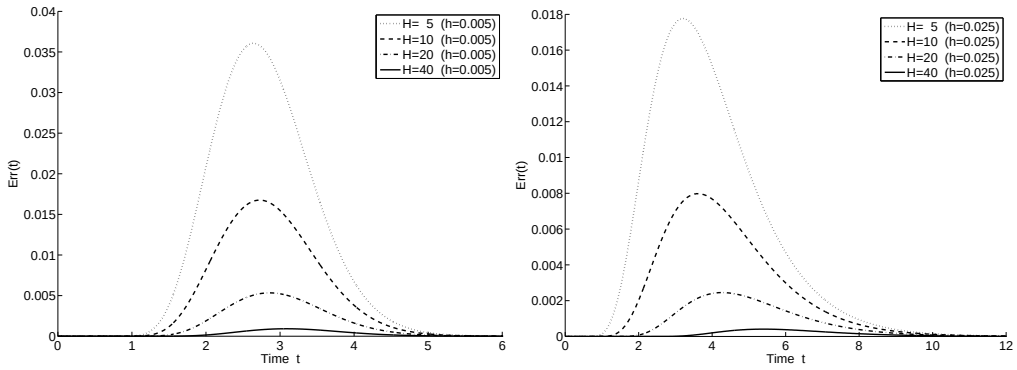

Figure 6: Maximal absolute error for a simulation with fixed parameters $a = 0.2$ and $\omega = 1.1$ (left $h_1 = 0.005$, right $h_2 = 0.025$). Notice the different scaling of the ordinates.

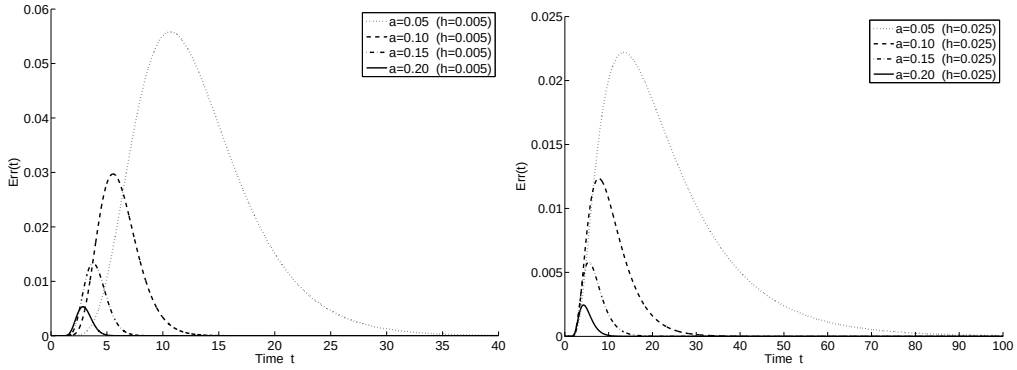

Figure 7: Maximal absolute error for a simulation with fixed parameters $H = 20$ and $\omega = 1.1$ (left $h_1 = 0.005$, right $h_2 = 0.025$). Notice the different scaling of the ordinates.

To achieve a qualitative evaluation of the errors we compare errors of our approximate ABC and non-reflecting *characteristic boundary conditions* (CBCs) [10, 11]. For the given D1Q2 model, the CBC method requires to solve the advection equation

$$\partial_t \rho(x,t) + a\partial_x \rho(x,t) = 0$$

at the boundary. To this end, we approximate the spatial derivative with a one-sided second order finite difference quotient, which gives the ODE

$$\partial_t \rho(x_N,t) = -\frac{a}{2h}\left[3\rho(x_N,t) - 4\rho(x_{N-1},t) + \rho(x_{N-2},t)\right].$$

Then in each iteration of the LBE, one step of the explicit Euler method is

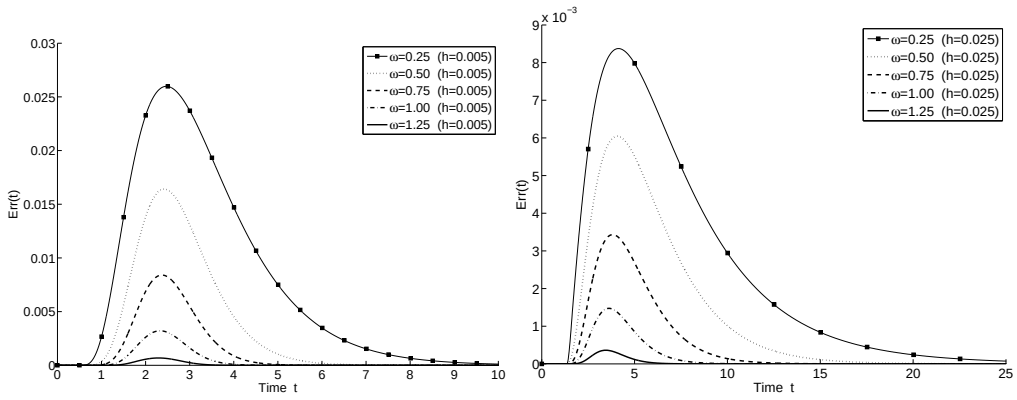

Figure 8: Maximal absolute error for a simulation with fixed parameters $H = 20$ and $a = 0.25$ (left $h_1 = 0.005$, right $h_2 = 0.025$). Notice the different scaling of the ordinates.

used to obtain ρ at the boundary:

$$\rho(x_N, t_k) = \rho(x_N, t_{k-1}) - \frac{a}{2}\left[3\rho(x_N, t_{k-1}) - 4\rho(x_{N-1}, t_i) + \rho(x_{N-2}, t_{k-1})\right].$$

This new macroscopic boundary quantity is transferred to the populations by an appropriate evaluation of the equilibrium distribution:

$$f_i(N, k) = \frac{1}{2}\rho(x_N, t_k)(1 + ac_i), \quad i = 1, 2.$$

We choose parameters to be $a = 0.15$, $\omega = 1.4$ and $h = 0.01$ and compare maximal absolute errors (27) for both boundary conditions in Fig. 9. We stress again that the approximate ABC can be arbitrarily accurate by increasing the maximal history depth H. For the given test case, a value of $H = 25$ is sufficient to obtain smaller errors compared to a CBC. In Fig. 9 one can see that the novel approximate ABC leads to smaller errors.

When comparing the plots of Figs. 6-8 with respect to the step size h (left and right plots each), one can see that the magnitude of the errors is different. Note the different scales of the axis. Strikingly, the errors are decreasing when the step size h is enlarged (compare left and right plots). A similar observation is possible when inspecting relative errors instead of absolute errors (27). Given a maximal history depth H and a step size h the boundary condition uses information from past boundary populations up to time $t = kh - 2Hh$. Hence, for the boundary condition (26) information from the time interval $[kh - 2Hh, (k-1)h]$ is used. Furthermore, the larger

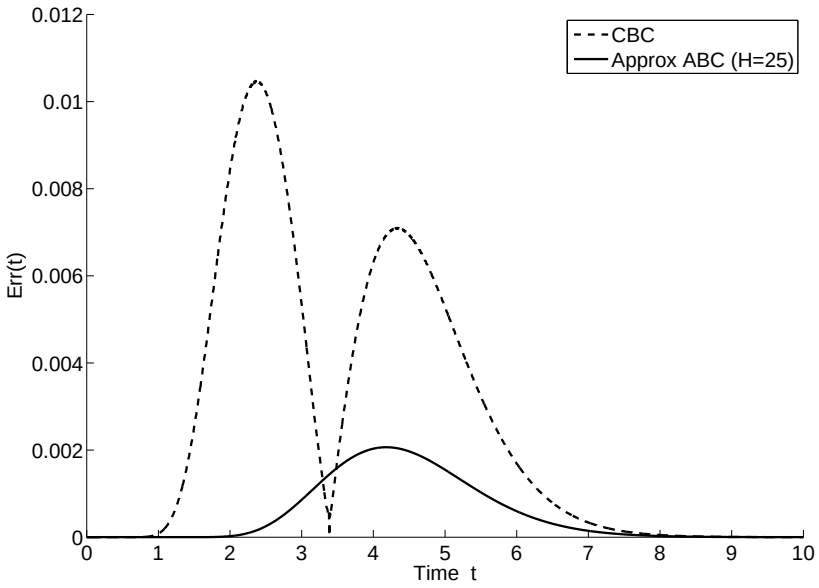

Figure 9: Comparison of absolute errors in CBC and the approximate ABC (with parameters $a = 0.15$, $\omega = 1.4$ and $h = 0.01$).

the spatial grid size h, the longer the employed history. This can explain the smaller errors for larger grid sizes (and step sizes). In order to see the dependence of the step size (grid size) in a more consistent manner, we choose the maximal history depth H according to the step size, such that the length of the interval remains constant, i.e.,

$$2Hh = C = \text{const.} \tag{28}$$

Since in the limit h to zero, the history depth has to tend to infinity, the approximate ABC tends to the exact ABC. Next, we show the results for two different choices of parameters a, ω as well as the constant C. The maximal relative error $\mathrm{Rel}(h)$ is given as

$$\mathrm{Rel}(h) := \max_t \left(\sum_{x \in G_x} r^h(x,t)^2 \right)^{1/2} \quad \text{with} \quad r^h(x,t) := \left| \frac{\rho^h(x,t) - \rho^h_{\mathrm{ref}}(x,t)}{\rho^h_{\mathrm{ref}}(x,t)} \right|,$$

where $r^h(x,t)$ is the local relative error and superscripts h indicate solutions computed on the lattice corresponding to step size h. In Figs. 10 and 11 the maximal relative error is plotted for different step sizes and we see the

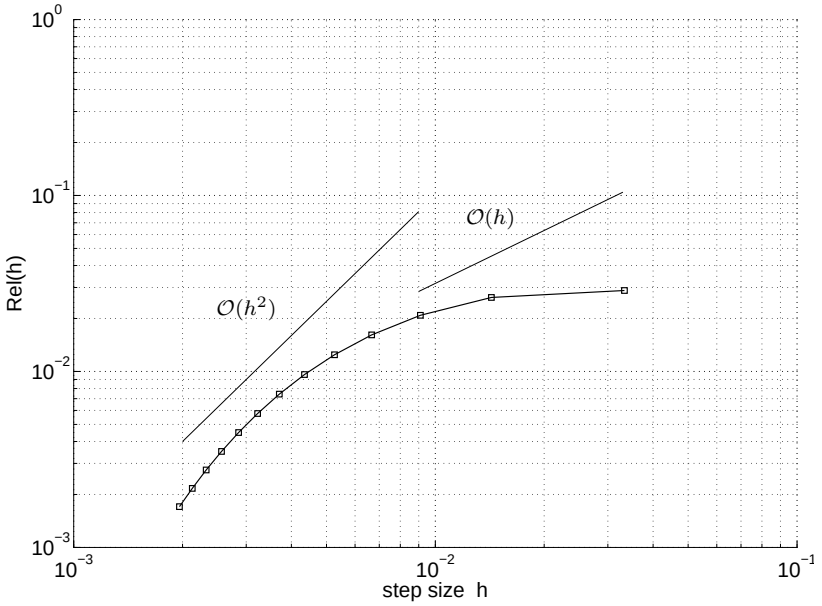

Figure 10: Maximal relative error for different step sizes h. Parameters in this simulation are: $a = 0.4$, $\omega = 0.3$ and $C = 0.3$

expected behavior: A smaller step size h results in a smaller relative error. For the parameter set of Fig. 10 the decay is as fast as of h^2. With the choice of parameters of Fig. 11 the decrease is even of order ten (and seems to increase further). For smaller step sizes to fulfill (28) the history depth H has to be increased. By this change we obtain a higher level of accuracy, therefore the error is plotted not only for different step sizes but indirectly also for boundary conditions of different levels of accuracy. This can explain the increasing slopes seen in Figs. 10-11.

6. Conclusions

In this article, we considered the lattice Boltzmann model D1Q2. First, we derived the evolution of populations depending on a set of nodes (which are feasible and sufficient), as for example initial values only. We showed how trees can be used to visualize the evolution of populations over several time levels: All paths of the tree have to be considered, since each path gives a path-dependent contribution. Then, this knowledge was used to construct an exact artificial boundary condition. The exact artificial boundary condition was based on the assumption that the exterior domain is in a homogeneous

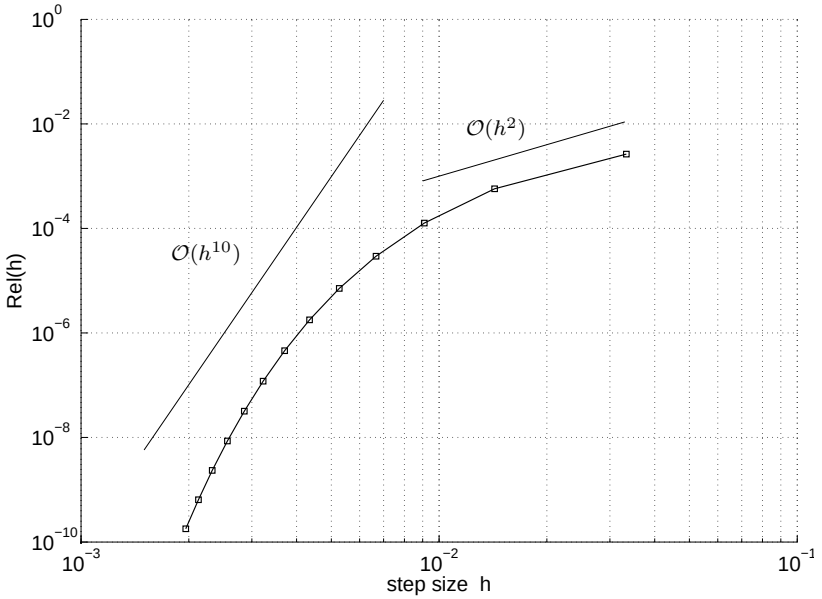

Figure 11: Maximal relative error for different step sizes h. Parameters in this simulation are: $a = 0.6$, $\omega = 1.1$ and $C = 0.1$

equilibrium at $t = 0$. To reduce the effort, an approximation to the exact boundary condition was derived. This approximation is based on a truncated history depth, where corresponding sums are truncated. In order to retain an equilibrium, we developed a general consistency condition.

Finally, we tested numerically the approximate artificial boundary condition. The error was compared to the exact artificial boundary condition, where we investigated and visualized its dependence on the model parameters (a and ω), the step size h and the maximal history depth H. The latter parameter H controls the level of accuracy of the approximation. A common approach of non-reflecting boundary conditions is to analyze characteristics of a hyperbolic PDE system. We made a numerical comparison of the approximate artificial boundary condition and characteristic boundary conditions and we showed that we can in fact improve upon the characteristic boundary condition.

The formulas of the exact artificial boundary condition can be interpreted as a convolution. Thus, another ansatz for an approximation may be given by employing sums of exponentials, cf. [16].

Furthermore, we plan to extend this first exact artificial boundary condi-

tion for the lattice Boltzmann method (D1Q2) to more advanced discretizations models. Thereby challenges will appear, such as a much higher number of paths or nonlinearities in the collision operator.

Acknowledgments

The authors are very grateful for fruitful discussions with Michael Junk from the University of Konstanz, Germany.

References

[1] D. Heubes, A. Bartel, M. Ehrhardt, An introduction to the lattice Boltzmann method for coupled problems, pp. 3–30 in [3].

[2] S. Succi, The lattice Boltzmann equation for fluid dynamics and beyond, Oxford University Press, Oxford, UK, 2001.

[3] M. Ehrhardt (Ed.), Progress in computational physics, Vol. 3, Novel trends in lattice-Boltzmann methods: Reactive flow, physicochemical transport and fluid-structure interaction, Bentham Science Publishers Ltd., 2013.

[4] D. Haydock, J. M. Yeomans, Lattice Boltzmann simulations of acoustic streaming, Journal of Physics A: Mathematical and General 34 (25) (2001) 5201–5213.

[5] C. Sun, L. L. Munn, Lattice-Boltzmann simulation of blood flow in digitized vessel networks, Computers & Mathematics with Applications 55 (7) (2008) 1594–1600.

[6] S. Geller, J. Tölke, M. Krafczyk, Lattice-Boltzmann method on quadtree-type grids for fluid-structure interaction. In: H.-J. Bungartz, M. Schäfers (Eds.), Fluid-structure interaction: Modelling, simulation, optimisation, Lecture Notes in Computational Science and Engineering, Vol. 53, Berlin, Germany, 2006.

[7] Y. Vanderhoydonc, W. Vanroose, C. Vandekerckhove, P. Van Leemput, D. Roose, Numerical lifting for lattice Boltzmann models, pp. 127–154 in [3].

[8] M. Tekitek, M. Bouzidi, F. Dubois, P. Lallemand, Towards perfectly matching layers for lattice Boltzmann equation, Computers & Mathematics with Applications 58 (5) (2009) 903–913.

[9] A. Najafi-Yazdi, L. Mongeau, An absorbing boundary condition for the lattice Boltzmann method based on the perfectly matched layer, Computers & Fluids 68 (2012) 203–218.

[10] S. Izquierdo, N. Fueyo, Characteristic nonreflecting boundary conditions for open boundaries in lattice Boltzmann methods, Physical Review E 78 (2008) 046707.

[11] D. Heubes, A. Bartel, M. Ehrhardt, Characteristic boundary conditions in the lattice Boltzmann method for fluid and gas dynamics, Journal of Computational and Applied Mathematics (2013), in press, 10.1016/j.cam.2013.09.019.

[12] Y. Qian, D. d'Humieres, P. Lallemand, Lattice BGK models for Navier-Stokes equation, Europhysics Letters 17 (6) (1992) 479–484.

[13] M. Junk, M. Rheinländer, Regular and multiscale expansions of a lattice Boltzmann method, Progress in Computational Fluid Dynamics 8 (2006) 25–37.

[14] P. L. Bhatnagar, E. P. Gross, M. Krook, A model for collision processes in gases. I. Small amplitude processes in charged and neutral one-component systems, Physical Review 94 (3) (1954) 511–525.

[15] S. Chapman, T. Cowling, The mathematical theory of non-uniform gases, Cambridge University Press, London, UK, 1970.

[16] A. Arnold, M. Ehrhardt, I. Sofronov, Discrete transparent boundary conditions for the Schrödinger equation: Fast calculation, approximation, and stability, Communications in Mathematical Sciences 1 (3) (2003) 501–556.